Passive acoustic records of seafloor methane bubble streams on the Oregon continental margin

R.P. Dziak[1], H. Matsumoto[2], R. W. Embley[1], S. G. Merle[2], T-K Lau[2], T. Baumberger[1], S. R. Hammond[3], N. Raineault[4]

[1]NOAA/Pacific Marine Environmental Laboratory, Hatfield Marine Science Center, Newport, OR 97386 U.S.A.

[2]Cooperative Institute for Marine Resource Studies, Oregon State University/NOAA, Hatfield Marine Science Center, Newport, OR 97365, U.S.A.

[3]Earth Resources Technology, Inc, Laurel, MD, 20707, U.S.A.

[4]Ocean Exploration Trust, 215 South Ferry Road, Narragansett, RI 02882. U.S.A.

1. Abstract

We present acoustic records of methane bubble streams recorded ~10 km southwest of Heceta Bank on the Oregon continental margin using an autonomous hydrophone. The hydrophone was deployed at 1228 m water depth via a Remotely Operated Vehicle (ROV) during the E/V *Nautilus* expedition (NA072) in June 2016. Bubble sound is produced by detachment of the gas bubble from the end of a tube or conduit which causes the bubble to oscillate, producing a sound signal. Despite persistent ship propeller and ROV noise, the acoustic signature of the overall bubble seep site can be seen in the hydrophone record as a broadband (1.0 – 45 kHz) series of short duration (~10-20 msec) oscillatory signals that occur in clusters lasting 2-3 secs. The frequency of an individual bubble's oscillation is proportional to the bubble's radius; estimates here of bubble radii are consistent with bubble sizes observed in ROV still images. Acoustic signal loss models imply bubble sounds might be recorded over an area of seafloor from ~300 – 3.2 x10^4 m^2. This study represents a first-step in attempting to identify and quantify deep-ocean bubble stream sounds using passive acoustic techniques.

Key words: Passive acoustics, methane seep, bubble streams, gas flux, E/V *Nautilus* Cruise ID NA072

2. Introduction

Marine methane is an important greenhouse gas that is stored as both an icy methane hydrate deposit, as well as a gas phase, within the sediment wedges of continental margins. Marine methane is created through biogenic and thermogenic processes within these sediments, and enters the water column through various pathways [Judd, 2003]. Moreover, marine methane can also have sources in a variety of continental margin geological settings, including natural gas seeps, gas hydrate deposits, and mud volcanoes [Salmi et al., 2011; Johnson et al., 2015].

However, there is much that remains unknown about the number and distribution of methane bubble seep emissions in the deep-ocean, which is certainly the case for the focus area of this study, the Oregon continental margin [Salmi et al., 2011; Johnson et al., 2015]. As with any deep-ocean phenomena, much remains unknown because of the lack of observations as well as the extreme difficulty in collecting sustained observations. Previous ocean seep research worldwide has sought to measure seafloor bubble seep fluxes using video imaging [Leifer and MacDonald, 2003; Mastepanov et al., 2008]], as well as active acoustics [Schneider von Deimling et al., 2010; Salmi et al., 2011], direct gas sampling and capture [Washburn et al., 2005; Leifer, 2015], and passive acoustics [Leifer and Tang, 2007]. Seafloor methane bubble streams have been shown to produce acoustic signals in the 1-10 kHz range with bubble sizes (measured from optical and acoustic methods) in the sub-millimeter to centimeter range [Leifer and Tang, 2007; Wiggins et al, 2015].

There has been much recent progress in making quantitative measurements of seafloor methane bubble streams using passive acoustics [e.g. Leifer and Tang, 2007; Salmi et al., 2011]. Passive acoustic monitoring offers several advantages over other methane bubble stream detection and monitoring techniques because it offers a relatively low-cost method that covers a wide area of the seafloor, and therefore multiple bubble stream sites can be detected and recorded [Wiggins et al., 2015]. Although passive acoustics does not allow for a direct measure of bubble size and shape as do video and active acoustics, current improvements in acoustic data logging technologies and storage allow for extended recording (hours to days) at very high sample rates (>200 kHz) enabling broadband characterization of the seep and ambient sound fields. Passive acoustic, long-term monitoring of bubble streams can be particularly useful since bubble streams can turn on and off frequently over time and over small spatial scales [Boles et al., 2001]. A notable example of passive acoustic monitoring of seafloor bubble streams is the use of the Ocean Observatories Initiative (OOI) cabled hydrophones monitoring the Hydrate Ridge seep field on the Oregon margin [OOI, 2016]. The OOI hydrophones, however, are set at a 200 Hz sample rate and therefore may be missing sounds produced by the bubble streams at high (>1 kHz) frequencies, making it difficult to comprehensively quantify marine seep behavior.

Another issue that makes using passive acoustic techniques to measure the sound of bubble streams a challenge are the high levels of background (ambient) noise. Man-made noise in the ocean is thought to have increased by a factor of 3-4 (or 9-12 dB) since the 1960s in areas near major shipping lanes like the Oregon margin. This increase is thought to largely be due to increases in vessel traffic transiting the world's oceans and an increase in the gross tonnage of ships used in the modern shipping fleet [Frisk et al., 2003; Hildebrand, 2009]. Moreover, the classic ocean sound study by Wenz (1962) showed that while ambient noise can be dominated by commercial shipping at low frequencies (< several hundred Hz), natural sources such as wind-generated waves dominate at high frequencies (> several hundred Hz). Thus wave noise is also in the bubble stream sound bandwidth, and therefore an ongoing obstacle to extracting clear methane bubble stream signals from a passive acoustic record of the seafloor soundscape are the ubiquitous anthropogenic and natural sources of ambient sound.

Here we report on the results of deploying a passive acoustic recorder within a bubble field ~10 km SW of Heceta Bank on the Oregon continental margin (Fig 1). The Oregon margin is within the Cascadia Subduction zone, where subduction causes compressive stress across the Oregon margin creating numerous faults that tap deep sources of methane-rich fluids [Kulm et al., 1986]. Although there have been many detailed studies of selected sites on the Oregon margin, the Oregon margin has not been systematically surveyed for methane seeps because there has not been an efficient technology to detect water-column bubble streams rising from the more vigorous deep-ocean seep sites. The goal of our study was to test the feasibility of passively recording the sounds of bubbles emanating from the deep seafloor of the Oregon margin and to gauge their frequency bandwidths. Moreover, we wanted to evaluate the quality of the recordings to see if subsequent spectral analysis could be used to characterize the range of bubble sizes using previously established bubble frequency to radius relationships.

3. Deployment and Acoustic Recording Methods

The SW Heceta bank site is at ~1228 m water depth and forms a broad, relatively shallow gradient plateau along the western edge of the Cascadia accretionary prism. The autonomous hydrophone was deployed in June 2016 within a seep field (Fig 2a) using the Ocean Exploration Trust ROV *Hercules* during the E/V *Nautilus* expedition NA072. The NA072 expedition used a Kongsberg EM302 multibeam sonar system to map bubble streams at a regional scale along the Washington, Oregon and northern California margins, followed by in situ investigation of bubble stream sites using the ROV *Hercules* [Embley et al., 2016]. After ~5 hrs on the bottom, the ROV deployed the hydrophone at the SW Heceta Bank site within an area of ubiquitous bubble stream activity that also held bacterial mats, clam beds and a tubeworm bush. Once the hydrophone was deployed, the ROV moved 1000-1200 m northeast of the hydrophone to explore another seep site and to reduce the amount of ROV hydraulic system and dynamic-positioning thruster noise recorded by the hydrophone.

The hydrophone used for this experiment was a Greenridge Sciences Acousonde 3B™. The Acousonde omnidirectional, record at a 232 kHz sample rate with a 6-pole linear phase anti-aliasing filter at 42 kHz, has an element sensitivity of -204 dB re 1 V/µPa for the high frequency channel with 49 dB flat gain above 25 Hz, and an estimated gain error of ±1 dB. The hydrophone was strapped to a concrete block which in turn anchored the hydrophone to the seafloor (Fig 2a). A positively buoyant float marked the location of the hydrophone, which recorded for ~12 hrs on the seafloor before being recovered and brought back to the surface vessel. The time duration of the deployment was limited to 12 hrs due to time constraints for use of the ROV. Figure 3 shows the spectrogram of the entire hydrophone record from the deployment, which includes the signals we interpret as sounds from the streams of bubbles emanating from the seafloor, as well as the noise from the ROV, transponders used for ROV navigation, and background noise once the hydrophone was on deck of the E/V *Nautilus*. The telepresence capability of the E/V *Nautilus*, which provided real-time ship-to-shore communication, permitted the science party on-land to interact with ship-based scientists to select the deployment site, discuss dive plan priorities and determine the most effective recording strategies for detecting bubble stream sounds. Samples of the bubbles were collected and analyzed for their gas compositions [Baumberger et al., 2017] and were found to be composed of >99% methane, with trace amounts of CO_2, nitrogen, argon, neon and helium.

4. Bubble Signal Characteristics

Previous research on the passive acoustics of seep bubble streams indicate sound is generated during bubble formation, where detachment of the gas bubble from the end of a tube or conduit causes the bubble to oscillate, producing sound [Minneart, 1933; Fig 2b]. This seep bubble oscillation, or sound formation, is thought to occur due to severing or pinching of the bubble at the end of a tube or conduit, and thus is similar to bubble formation from a capillary tube [Vazquez et al., 2005; Leifer and Tang, 2007]. There are two end member bubble stream plumes based on gas flow rates and bubble sizes, the first are low gas flow rates that produce plumes with a small range of bubble sizes that follow a Gaussian distribution. These are referred to as minor seeps [Leifer and Boles, 2005a]. The second are high flow plumes that produce bubbles by a turbulent jet and are characterized by bubble size distributions that follows a power law [Leifer and Boles, 2005a; Leifer and Culling, 2010]. The sound from a turbulent jet stream is formed by overlapping of bubble sounds of various frequencies (from various sized bubbles), and thus sound scattering and coupling can shift the bubble frequencies [Vazquez et al., 2005; Leifer and Tang, 2007; Wiggins et al., 2015]. Hydrate plates may also enclose bubbles, increasing their lifetime in the water-column and the time duration of oscillatory behavior [Rehder et al., 2002], although the bubble acoustic source is thought to persist for only a few cycles, dampening very rapidly [Leifer and Tang, 2007]. Direct observations via the ROV indicate the SW Heceta Bank seep site (where there are clusters of bubble streams) can be described as a low flow rate field. As bubbles form in low flow bubble streams, each bubble can generate a sound whose peak frequency, *f*, (or zeroth oscillatory mode) is inversely proportional to the bubble equivalent spherical radius, *r*, under a hydrostatic pressure, P_A, given by the equation [Minnaert, 1933]:

$$f = \frac{1}{2\pi r}\sqrt{\frac{3\gamma P_A}{\rho}} \qquad (1)$$

where, ρ is seawater density, and γ is the heat capacity ratio for methane, which is ~1.32 [Wiggins et al., 2015]. Therefore using the acoustic record of the bubble sounds we may be able to approximate the range of bubble sizes within a stream. Moreover, it may also ultimately be possible to use the hydrophone estimate of bubble radii to gauge the volume of methane being released at these seafloor seep sites. Thus the hydrophones may potentially allow us to constrain the non-dissolved, gaseous amounts of methane emanating from the seafloor. Although it should be noted that this method will not allow for assessment of the amount of emitted methane from advective flux of dissolved methane that does not produce sound.

Figures 4a and 4b show focused spectrograms derived from 225 sec of the hydrophone data using the full bandwidth, and 8 sec of hydrophone data over a narrower bandwidth. Although there is considerable background noise on the record sourced from the surface ship propeller and ROV hydraulic noise in the area, as well as the ultra-short baseline (USBL) transponder used to navigate the ROV, there appears to be several examples of continuous broadband sounds with frequency ranges of ~5 to 35 kHz and durations of 2-3 secs. These signal packets have fairly abrupt onsets and are ~10-20 dB above background noise levels, although their low frequencies, starting at under 10 kHz, are lost in the mechanical noise. We interpret these signal packets as likely being produced by plumes of methane gas bubbles emanating from the seafloor, where the duration and frequency of packets are consistent with bubble-sound formation models.

Example time-series of the short duration (~10 msec) oscillatory waveforms of the bubble generated signals are shown in Figures 5,b. These signals occurred within the broadband frequency range of the spectra in Figure 4 interpreted as the bubble stream signals. To add confidence and further quantify our visual identification of these bubble oscillation signals, we calculated a short-term/long-term averages (5 msec and 3 sec time windows, respectively) on these sections of the hydrophone time-series. The optimal window length and detection threshold used here are based on the frequency content of the desired signals [Withers et al., 1998; Trnkoczy, 2002], where the short-term average window should be less than the shortest event signals that are expected to be captured, and the long-term average window should be longer than a few periods of background noise fluctuations. In this case, the individual oscillation signals are ~5-10 msec in length, however the total duration of the combined stream of bubble signals observed in the spectra are 2-4 secs (Fig 4b).

Typical detection thresholds using short-term/long-term average (sta/lta) ratios for a quiet seismic site are 2-4 times above background levels [Trnkoczy, 2002]. This SW Heceta bank seep hydrophone record has sta/lta normalized background levels of ~0.1. The heavy lines in Figures 5c,d highlight the waveform amplitudes that exceed a threshold value of 0.2 of the normalized sta/lta., and thus a detection threshold of twice the normalized sta/lta ratio appears to clearly detect the oscillatory bubble signal packet from background sound. Despite these signal detection efforts, we still acknowledge there is uncertainty in the interpretation of these signals as caused by bubble oscillations. However, the similarity in frequency-time structure of the SW Heceta bank bubble signals to analogous bubble signals observed in previous studies [Vazquez et al. 2005; Leifer and Tang, 2007], and the clarity of these signals above background sound levels, suggests to us that there is a reasonable degree of confidence that these signals identified from SW Heceta bank hydrophone record are sourced from the methane bubbles emanating from the seafloor.

To improve identification of the low frequency end of the bubble signal packet, we applied a simple pre-whitening signal processing technique to enhance the bubble stream spectra. Figure 6 shows the acoustic data spectra shown in Figure 4b after the enhancement was applied. The technique involves selecting a 60-sec long segment of typical background noise from the hydrophone time series that does not include the bubble sounds and is in between the UBSL pings. The inverse of the magnitude of the background noise spectrum was then multiplied to the signal spectrogram. Thus in essence we are applying an inverse filter of [1/n(f)] to the bubble stream record, where n(f) is the short-term background noise without bubble sounds. Although our signal enhancement method is a relatively straightforward approach, Figure 6 illustrates that this technique does raise signal to noise ratios for the low frequency sections of the bubble stream data. The bubble stream sounds appear at a minimum to be ~20-40 dB above background noise levels, and the bubble sounds can be observed above background noise with some confidence down to 1 kHz. Thus, based on Figures 5 and 6, we interpret the bubble stream sound bandwidth to range from ~1 to 45 kHz.

5. Acoustic Estimates of Bubble Size

Transmission loss and detection radius

After identifying the bubble sound bandwidth from the hydrophone data, we next used equation (1) to estimate the bubble radii. We initially deployed the hydrophone within a field of observed seafloor bubble streams and sources to ensure we recorded bubble sounds. However, it seems necessary to also consider how large of an area of seafloor it would be possible for the hydrophone to detect bubble sounds, because it is also likely we recorded sounds of bubbles at a greater distance from the hydrophone that were outside the ROV's field of view during the deployment. To address this acoustic detection issue, we reviewed published transmission loss models (Fig 7; Won and Park, 2012). Acoustic waves emitted from a source in the ocean undergo attenuation in signal strength as they propagate. If spherical spreading is assumed, the loss in acoustic wave signal strength, or transmission loss (*TL*), becomes [Kinsler, et al., 1999]:

$$\mathrm{TL}=20 \log d+\alpha\cdot d \qquad (2)$$

where d represents the distance between acoustic source and receiver, and α is the acoustic absorption coefficient, which is highly frequency dependent. Figure 7 shows the acoustic transmission loss with distance and frequency. Transmission loss on a dB scale is proportional to the logarithm of distance up to 100 m. However, when distance exceeds 100 m the transmission loss increases exponentially as a result of the second term of equation (2), or the product of distance and the acoustic absorption coefficient. High frequency acoustic waves have even higher transmission loss due to a higher absorption with distance. Therefore, given the bubble acoustic received levels appear to be ~20-40 dB re $\mu Pa^2/Hz$ above background noise levels (Fig. 6), the loss models (Fig. 7) imply the bubble signal is sourced at maximum distances of ~10-100 m for a 1 kHz and 45 kHz bubble signals. Using these distances as acoustic detection radii suggests then that the bubble sounds were detected from an area of seafloor between ~300 – 3.2 x10^4 m^2 around the hydrophone.

The ROV USBL transponder pings provide a means to gauge these estimated bubble sound levels. The transponder (LinkQuest Inc. Tracklink 5000MA) produces short duration acoustic bursts (pings) with source levels of ~183 dB re $\mu Pa^2/Hz$ over a 14-20 kHz band. The hydrophone records show these transponder pings are as high as 80-100 dB re $\mu Pa^2/Hz$ above the lowest ambient noise levels (Fig. 6). The pings shown in Figure 6 were recorded when the ROV was at a range of ~1400 m from the hydrophone. The attenuation curves in Figure 7 indicate the signal transmission loss for the transponder pings should be ~65-70 dB at that distance. This is consistent with the received sound levels of the pings shown in Figure 6 and gives us confidence that the bubble sounds levels and area of detection we estimate are reasonable.

Bubble radii and volume

Using equation (1), we estimated bubble radii by assuming the frequency bandwidth recorded in Figure 6 of 1-45 kHz. As previously stated, the composition of the gas bubbles was measured at >99% methane [Baumberger et al., 2016], which means the gas specific heat (constant pressure and volume to use in equation (1) is ~1.32 [Wiggins et al., 2015]. Moreover, hydrostatic pressure at 1228 m is 1.25 x 10^7 Pa, the water density was measured at 1033.1 kg-m^{-3}, ocean water temperature at the seafloor was 2.92° C. Using these values in equation (1) yields estimates of bubble radii of 0.08 ± 0.01 to 3.48 ± 0.2 cm for 45 kHz and 1 kHz bubble signals, respectively. The uncertainty in radii estimates was derived from the frequency resolution of the spectrogram, which is 57.3 Hz/pixel. Figure 8a shows the bubble radius to frequency relationship given by equation (1). The largest values for radius are all under 20 kHz, becoming asymptotic as the frequency increases to 45 kHz. Thus these frequency based bubble radii estimates show a wide range of bubble sizes, from less than a millimeter (highest frequency) to several centimeters (lowest frequency). The bubble radii estimates in the centimeter range are consistent with bubble sizes observed in the ROV still images. Radii on the order of millimeters are more difficult to ground-truth on the still images, and is at the limits of the available image resolution.

We then estimated the cumulative bubble volume by using the radii estimates and assuming the bubbles have a roughly spherical volume that can be defined by $4/3\ \pi\ r^3$. The cumulative bubble volumes are shown in Figure 8b, where the total volume over the 1-45 kHz band is 0.022 ± 0.001 m^3. As can be seen in Figure 8b, the total volume estimate is dominated by the lower frequencies, where the total volume between 1-12 kHz is 0.0214 ± 0.001 m^3 (~21.4 ± 1.2 liters) and the remaining volume estimated from 12.1-45 kHz is 5.7 x 10^{-4} ± 3.2 x 10^{-5} m^3 (~0.57 ± 0.03 liters). These total bubble volume estimates are an order of magnitude larger than previous estimates based on video and active acoustic techniques [Leifer, 2010; Salmi et al, 2011]. This may be due to the larger area of seafloor that is measured using passive techniques, or simply due to the uncertainty in the empirical method employed here. However, these previous estimates were also made at sites that differ from SW Heceta Bank in both water depth and geological environment (60 m water off southern California and 150 m at Cascadia margin, Leifer, 2010 and Salmi et al., 2011, respectively). These environmental differences could also play a role in the discrepancy in volumes observed. Nevertheless, we think presenting these volume estimates has value in that it provides a first step in estimating the rates of methane bubbles being released at SW Heceta Bank. Nevertheless we also realize more rigorous acoustic and video sampling methods will be required in future experiments to better constrain methane volume release.

6. Summary

A 232 kHz sample rate hydrophone was deployed using an ROV within a bubble stream seep-site at ~1228 m depth on the Oregon continental margin. The hydrophone appears to have successfully recorded the oscillatory sound of bubbles emanating from the seafloor. Following signal processing of the acoustic record, the sound of the bubble streams can be seen as a broadband (1- 45 kHz) series of short duration (~0.2-0.5 msec) pulses that occur in clusters of dozens of pulses lasting 2-3 secs. The low frequency (<1 kHz) end of the bubble sounds is not clearly defined because that part is obscured by surface ship and local ROV noise. Acoustic signal loss models imply bubble sounds could be recorded over an area of seafloor between ~300 – 3.2 x10^4 m^2. Lastly, our estimates of the bubble radii are consistent with bubble sizes observed in the ROV still images.

It was our goal here to show that passive acoustic techniques can be used to record sounds produced by seafloor bubble streams. Although passive acoustic recorders often are fixed spatially, acoustic recorders can allow for long-term recording of sound energy over a wide spatial ranges allowing for monitoring of seep activity over a much larger area of the seafloor. In later experiments when we can better constrain background noise levels, bubble sound source levels, and distance to bubble sources, then we hope to provide better estimates of bubble gas volume, what the influence of ocean tides might be on the streams, and perhaps even estimates of seafloor gas flux.

7. Acknowledgments

Thanks to the NOAA Office of Ocean Exploration and Research, the Ocean Exploration Trust, as well the Captain and crew of the E/V Nautilus and ROV Hercules for making this experiment possible. We also thank B. Burgess of Greeneridge Sciences for providing information on the Acousonde's pre-amp gain curve and anti-aliasing filter, and two anonymous reviewers for their helpful comments that improved the manuscript. This paper is NOAA/PMEL contribution #4639.

8. References

Baumberger T., R.W. Embley, S.G. Merle, M.D. Lilley, N.A. Raineault, and J.E. Lupton (2017), Mantle derived helium and multiple methane sources in gas bubbles seeping from the Cascadia Continental Margin, submitted G-cubed.

Bernstein L, Bosch P, Canziani O, Chen Z, Christ R, & Riahi K (2008). *IPCC, 2007: Climate Change 2007: Synthesis Report.* Geneva: IPCC. ISBN 2-9169-122-4Judd, A.G. (2003). The global importance and context of methane escape from the seabed. Geo-Mar Lett. 23: 147. doi:10.1007/s00367-003-0136-z.

Boles, J.R., Clark, J.F., Leifer, I., and L. Washburn (2001)., Temporal variation in natural methane seep rate due to tides, coal oil point area, California. J. Geophys. Res.- Oceans, v:106, 27077-27086.

Embley, R.W., S.G. Merle, T. Baumberger (2016), Eos Transactions, American Geophysical Union.

Frisk, G., Bradley, D., Caldwell, J., D'Spain, G., Gordon, J., Hastings, M., Ketten, D. (2003). *Ocean noise and marine mammals*, (O. S. Board, Ed.) National Academy of Sciences, Washington, DC, 3rd ed., 221 pp.

Hildebrand, J. A. (2009). Anthropogenic and natural sources of ambient noise in the ocean, Mar. Ecol. Prog. Ser., 395, 5–20. doi:10.3354/meps08353.

Johnson, H. P., U. K. Miller, M. S. Salmi, and E. A. Solomon (2015), Analysis of bubble plume distributions to evaluate methane hydrate decomposition on the continental slope, Geochem. Geophys. Geosyst., 16, 3825–3839, doi:10.1002/2015GC005955.

Kinsler, L.E., A.R. Frey, A.B. Coppens, J.V. Sanders (1999). Fundamentals of Acoustics. 4th Edition, Wiley Pubs.

Kvenvolden, K.A. and B.W. Rogers (2005). Gaia's breath – global methane exhalations. Mar. Petro. Geo., v:22, 4 579-590.

Kulm, V. (1986). Oregon Subduction Zone: venting, fauna, and carbonates. Science, 231, p. 561.

Leifer, I., J. R. Boles, B.P. Luyendyk, J.F. Clark (2004). Transient discharges from marine hydrocarbon seeps: spatial and temporal variability. Environ. Geo., v:46, 8, 1038-1052.

Leifer, I. and J. Boles (2005). Measurement of marine hydrocarbon seep flow through fractured rock and unconsolidated sediment. J. Mar. Petrol. Geol., v:22, 4, 551-568.

Leifer, I. and D. Tang (2007). The acoustic signature of marine seep bubbles. J. Acous. Soc. Am., v:121, 1, DOI: http://dx.doi.org/10.1121/1.2401227.

Leifer, I. (2010). Characteristics and scaling of bubble plumes from marine hydrocarbon seepage in the Coal Oil Point seep field. J. Geophys. Res., v:115, doi:10/1029/2009JC005844.

Leifer, I., and Culling, D. (2010). Formation of seep bubble plumes in the coal oil point seep field. Geo-marine Lett., v:30, 3-4, 339-353.

Leifer, I. (2015). Seabed bubble flux estimation by calibrated video survey for a large blowout seep in the North Sea. J. Mar. Petrol. Geol., v:68,

Mastepanov, M., Sigsgaard, C., Dlugokencky, E.J., Houweling, S., Strom, L., Tamstorf, M.P., Christensen, T.R. (2008). Large tundra methane burst during onset of freezing. Nature, 456, 7222, 628-630.Minneart, M. (1933). On musical air bubbles and the sound of running water. Philos Mag., 16, 235-248.Rehder, G., P.W. Brewer, E.T. Peltzer, and G. Friedrich (2002). Enhanced lifetime of methane bubble streams within the deep ocean. Geophys. Res. Lett., v:29, 15, 1731. DOI:10/1029/2001GL013966.

Minneart, M. (1933). On musical air-bubbles and the sound of running water Philos. Mag., v:16, 104, 235-248.

Ocean Observing Initiative (2016). Southern Hydrate Summit 1 Seafloor, http://oceanobservatories.org/site/rs01sum1/

Salmi, M.S., H. P. Johnson, I. Leifer, J.E. Leister (2011). Behavior of methane seep bubbles over a pockmark on the Cascadia continental margin. Geosphere, v:7, 6, p1273-1283.

Schneider von Demling, J., Greinert, J., Chpamn, N.R., Rabbel, W., Linke P. (2010). Acoustic imaging of natural gas seepage in the North Sea: Sensing bubbles controlled by variable currents. Limnol. Oceanogr. Methods, v:8, 1960, 155-171.Trnkoczy, A. (2002), Understanding and parameter setting of sta/lta trigger algorithm, in *IASPEI New Manual of Seismological Observatory Practice. Volume 1*, edited by P. Bormann, p. IS 8.1, GeoForschungsZentrum, Potsdam.

Vazquez, A., Sanchez, R.M., Salmas-Rodrigues, A., Soria, A., Mansasseh, R. (2005). A look at three measurement techniques for bubble size distribution. Exp. Therm. Fluid. Sci., v:30, 49-57.

Washburn, L., J.F. Clark, Kyriakidis, P. (2005). The spatial scales, distribution, and intensity of natural marine hydrocarbon seeps near coal oil point, Calirfornia. Mar. Petrol. Geol., v:22, 4, 569-578.

Wenz, G. M. (1962). Acoustic ambient noise in the ocean: Spectra and sources. J. Acoust. Soc. Am. 34, 1936–1956.

Wiggins, S.M., I. Leifer, P. Linke, and J.A. Hildebrand (2015). Long-term acoustic monitoring at North Sea well site 22/4b. J. Mar. Petrol. Geol., v:68, 776-788.

Withers, M., R. Aster, C. Young, J. Beiriger, M. Harris, S, Moore, J. Trujillo (1998). A comparison of select trigger algorithms for automated global seismic phase and event detection. Bull. Seism. Soc. Am., v:88, No. 1, 95-106.

Won, T-H and S-J Park (2012). Design and implmentation of an omni-directional underwater acoustic micro-modem based on a low-power micro-controller unit. Sensors, v:12, 2, 2309-2323.

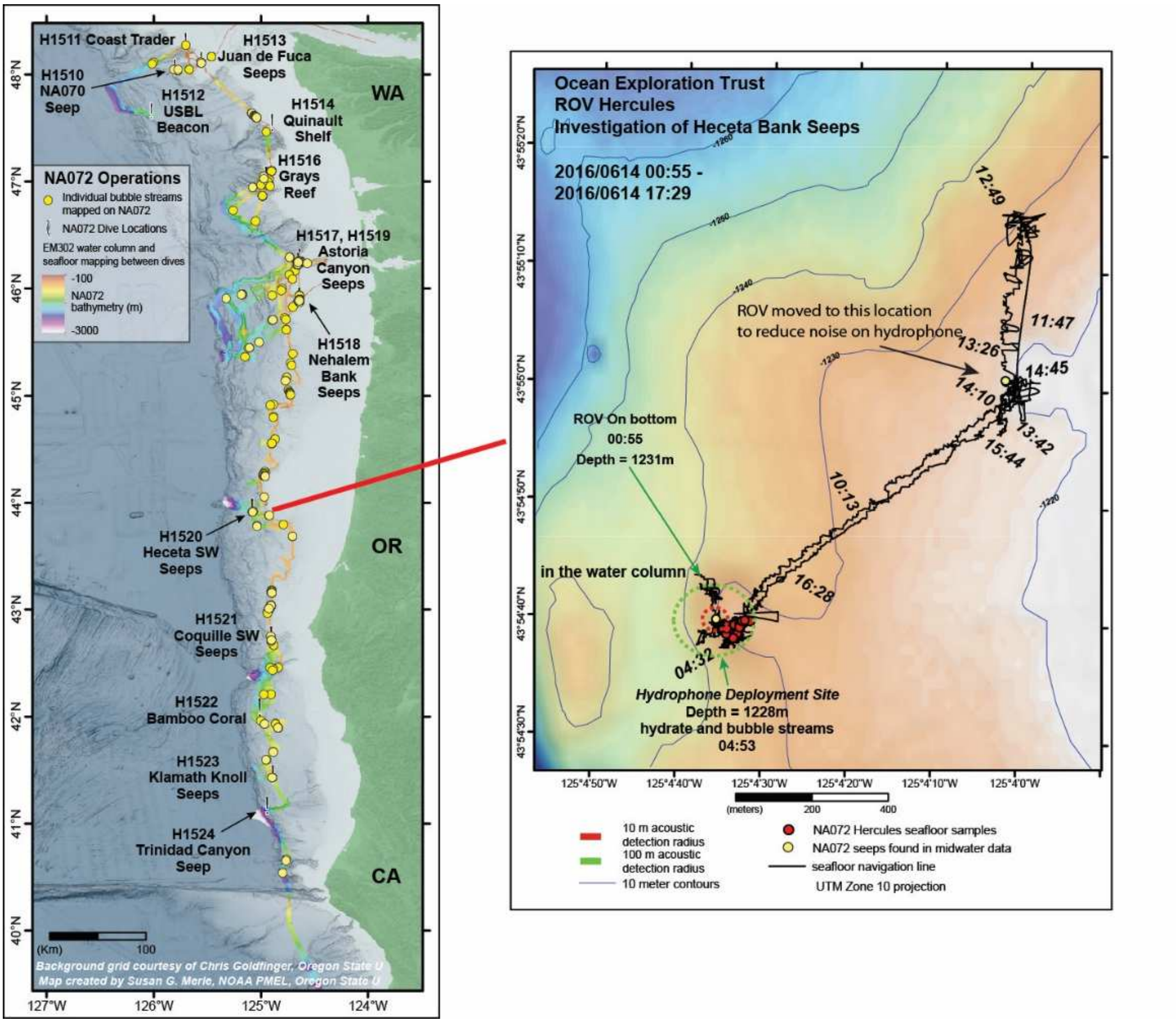

Figure 1: (Left) Map showing bathymetry and location of the SW Heceta Bank seep site, on the Oregon continental margin, as well as the other named locations of bubble seep sites mapped during the E/V *Nautilus* NA072 expedition. (Right) Track of Remotely Operated Vehicle (ROV) *Hercules* during deployment of hydrophone at SW Heceta Bank bubble seep site. The term "seep site" used in this study refers to a cluster of individual bubble streams within a few hundred meter radius area of the seafloor [Johnson et al., 2015]. Timing of ROV and activity of operations during deployment are labelled. Red and green dashed circles shows 100 and 1000 m transmission loss radius discussed in Figure 7

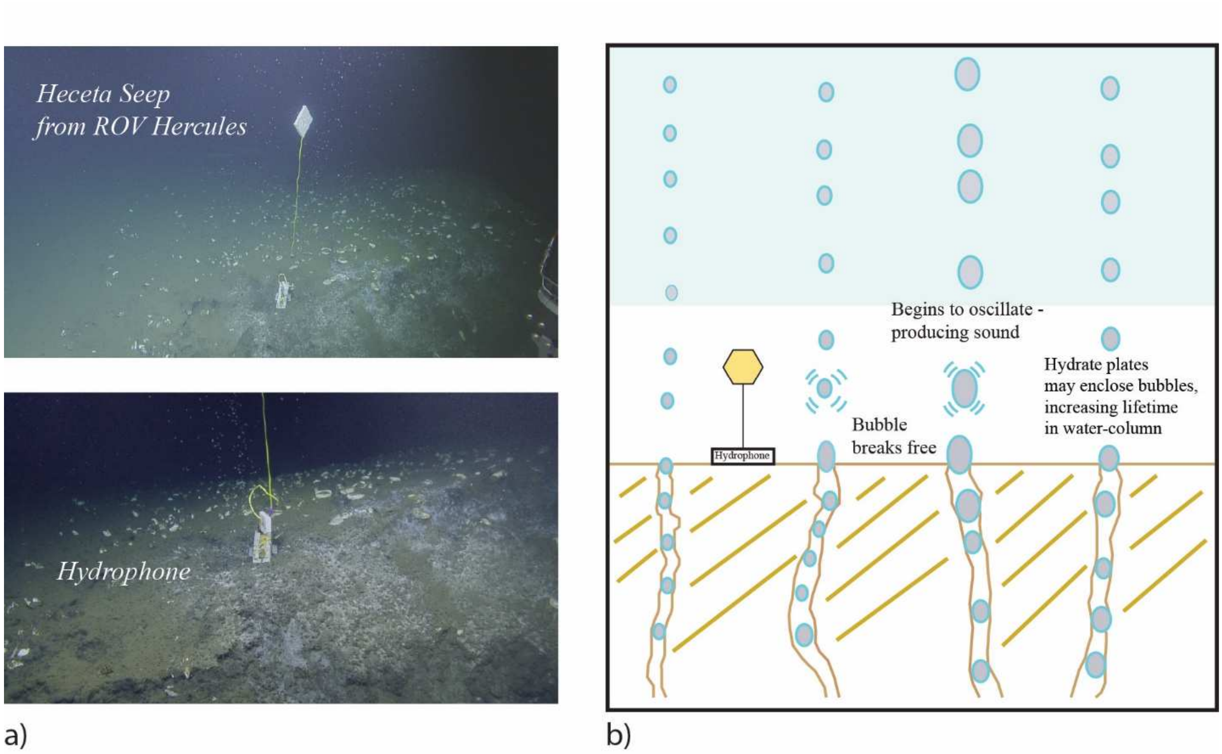

Figure 2: (a) Remotely Operated Vehicle pictures of hydrophone and float in a field of bubble streams at the SW Heceta Bank seep site shown in Figure 1. (b) Schematic showing flow of methane bubbles from sub-seafloor conduits into the water-column (based on Minneart, 1933). Oscillation of bubbles caused by detachment at the seafloor conduit leads to sound production.

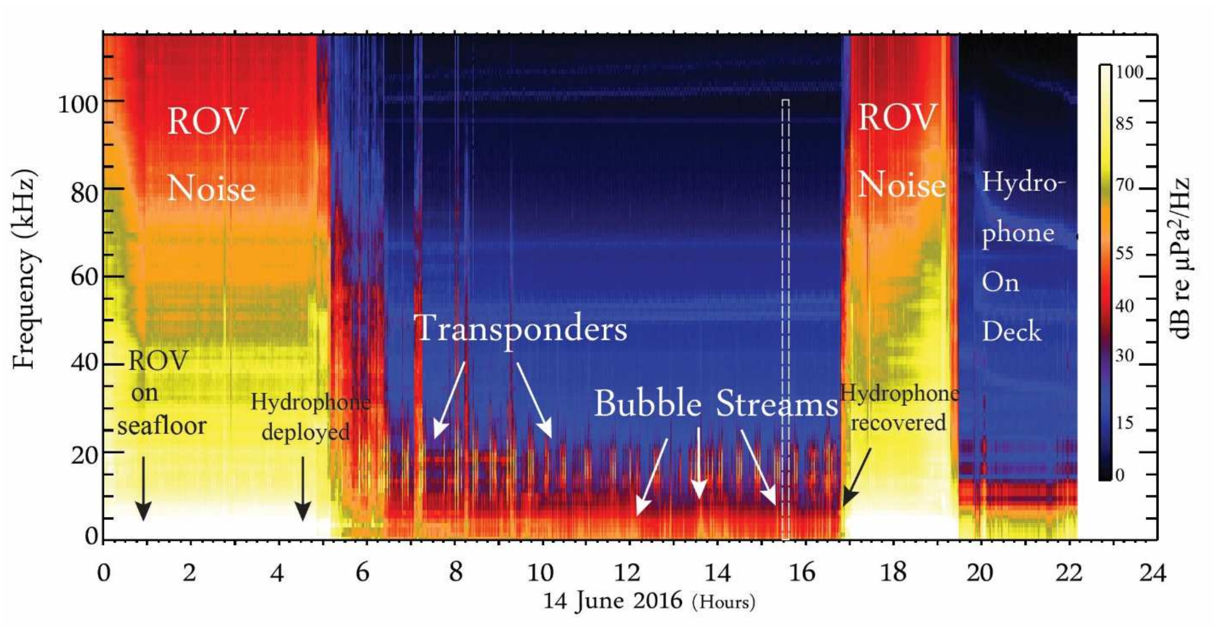

Figure 3: Shows the spectrogram of the entire hydrophone record deployed by a Remotely Operated Vehicle (ROV) at SW Heceta Bank. Arrows point to the various signals seen in the record, which includes the sounds from the bubble streams emanating from the seafloor, the noise from the ROV, the transponders used for ROV navigation, and the background noise recorded by the hydrophone once on the deck of the surface ship. Also labelled are the times the ROV was first on the seafloor, and when the hydrophone was deployed and recovered by the ROV. White dashed rectangle shows time and bandwidth of hydrophone spectra shown in Figures 4a,b.

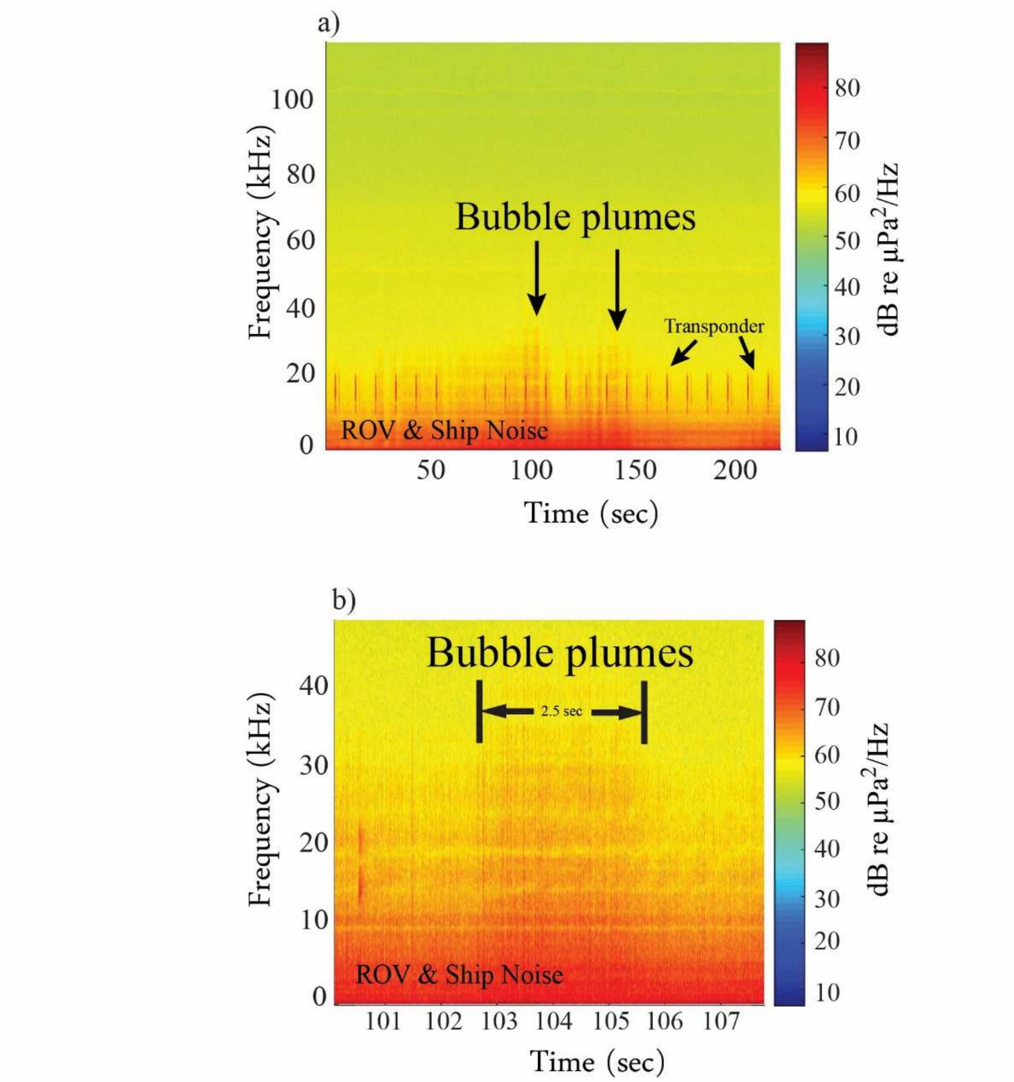

Figure 4: Spectrograms of hydrophone record from SW Heceta Bank. a) 225 second of hydrophone data over the 116 kHz band. Signature of bubble streams are labelled. Transponder pings used for ROV navigation are significant part of the record. ROV and ship propeller noise dominate record 1-5 kHz. Bubble stream sounds can be seen as broad band sounds in between transponder pings. b) Smaller scale sound spectra covering 6 second time period and 40 kHz. Spectral trace of bubbles appears as the 2.5 sec long band of energy in the 10-40 kHz range.

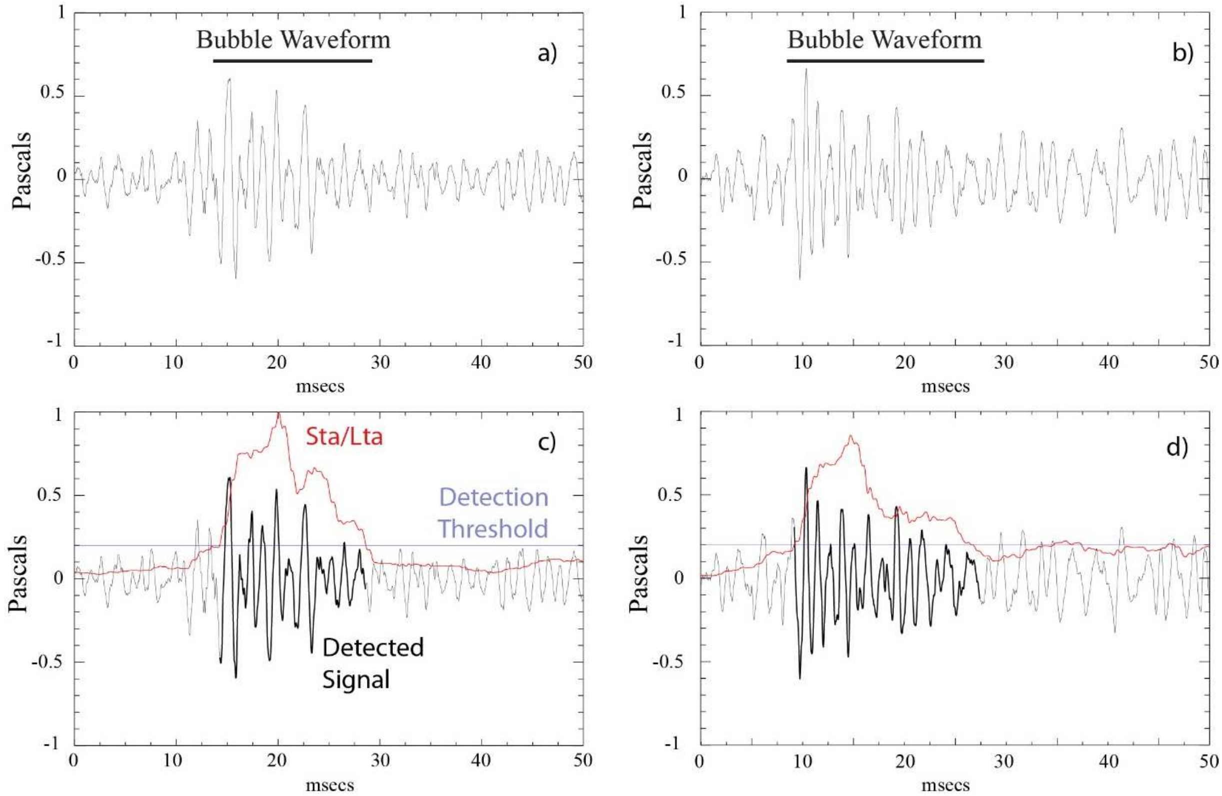

Figure 5: Examples of acoustic signals showing oscillatory sound from individual bubbles in the hydrophone record. The signals were filtered (0.4 – 11 kHz pass band) to reduce ship and ROV noise. Time series in (a) and (b) show likely bubble oscillation signals recorded 1 hour apart on 14 June 2016, 0600-0700z. Figures (c) and (d) illustrate signal detection methods used to further support visual identification of bubble signal packets. Red lines show short-term/long-term average ratio (5 msec/3.0 sec window lengths, respectively) of time series in (a) and (b). Heavy black line highlights segment of time series with detected bubble signal. Bubble signals were identified where sta/lta ratio exceeded 0.2 (purple line, normalized). Optimal window length and detection threshold used here are based on frequency content of tracked signals [Withers et al., 1998; Trnkoczy, 2002].

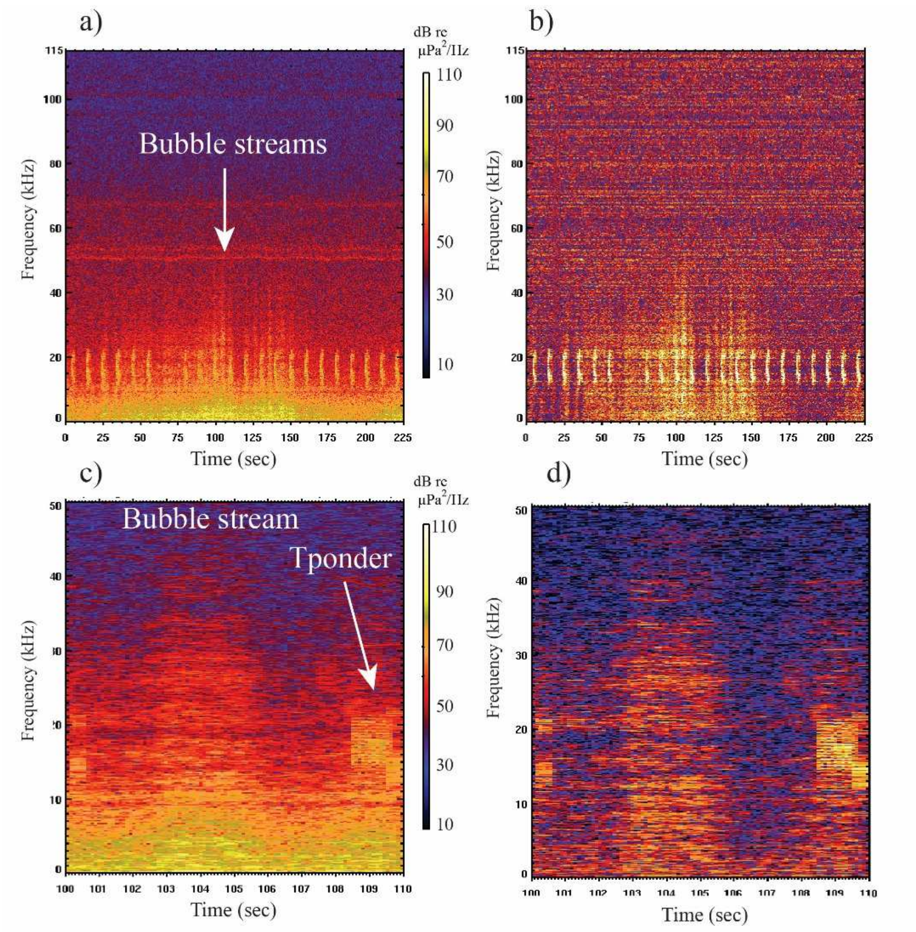

Figure 6: Background noise removal technique applied to acoustic data spectra shown in Fig 4b. The technique involves selecting a 60-sec long segment of typical background noise that does not include bubble sounds and is in between the UBSL pings. The noise spectrogram was then removed from the signal spectrogram. (a) and (c) show before noise reduction (over long and short periods of time), (b) and (d) show after noise reduction applied. The technique does appear to raise signal relative to noise for the low frequency sections of the bubble stream data, and shows bubble sounds can be observed above background noise down to 1 kHz.

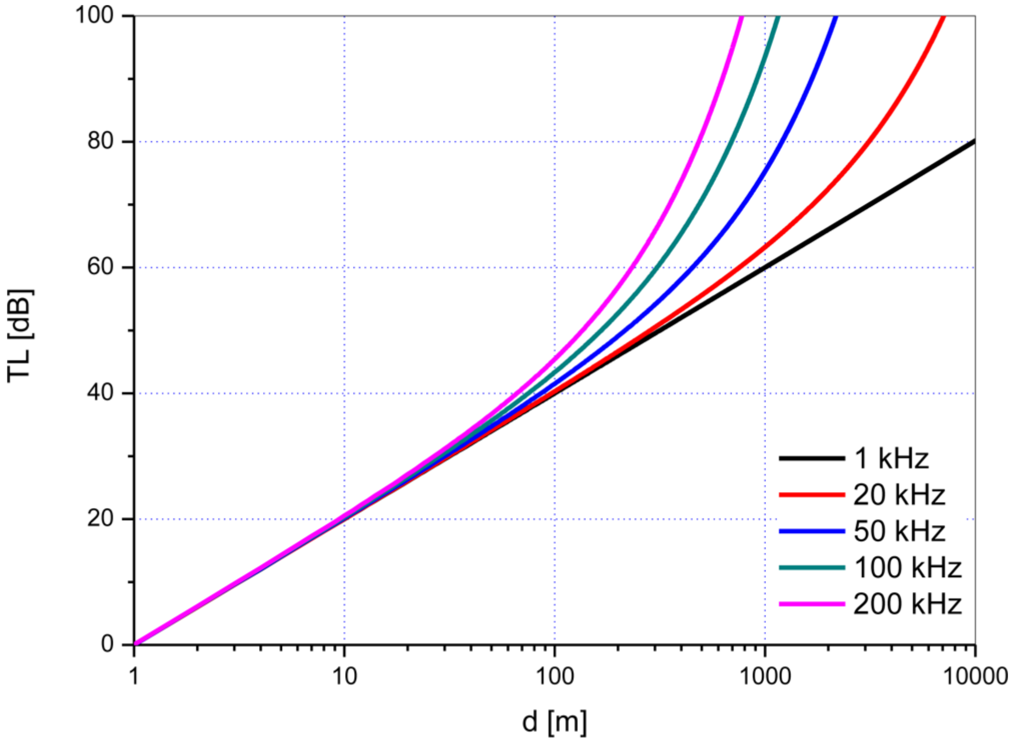

Figure 7: Acoustic signal (transmission) loss with distance and frequency. Transmission loss on a dB scale is proportional to the logarithm of distance up to 100 m. When distance exceeds 100 m, the transmission loss increases exponentially. Spherical spreading in sea water is assumed, with temperatures of 10 degrees Celsius. Image after Won and Park (2012).

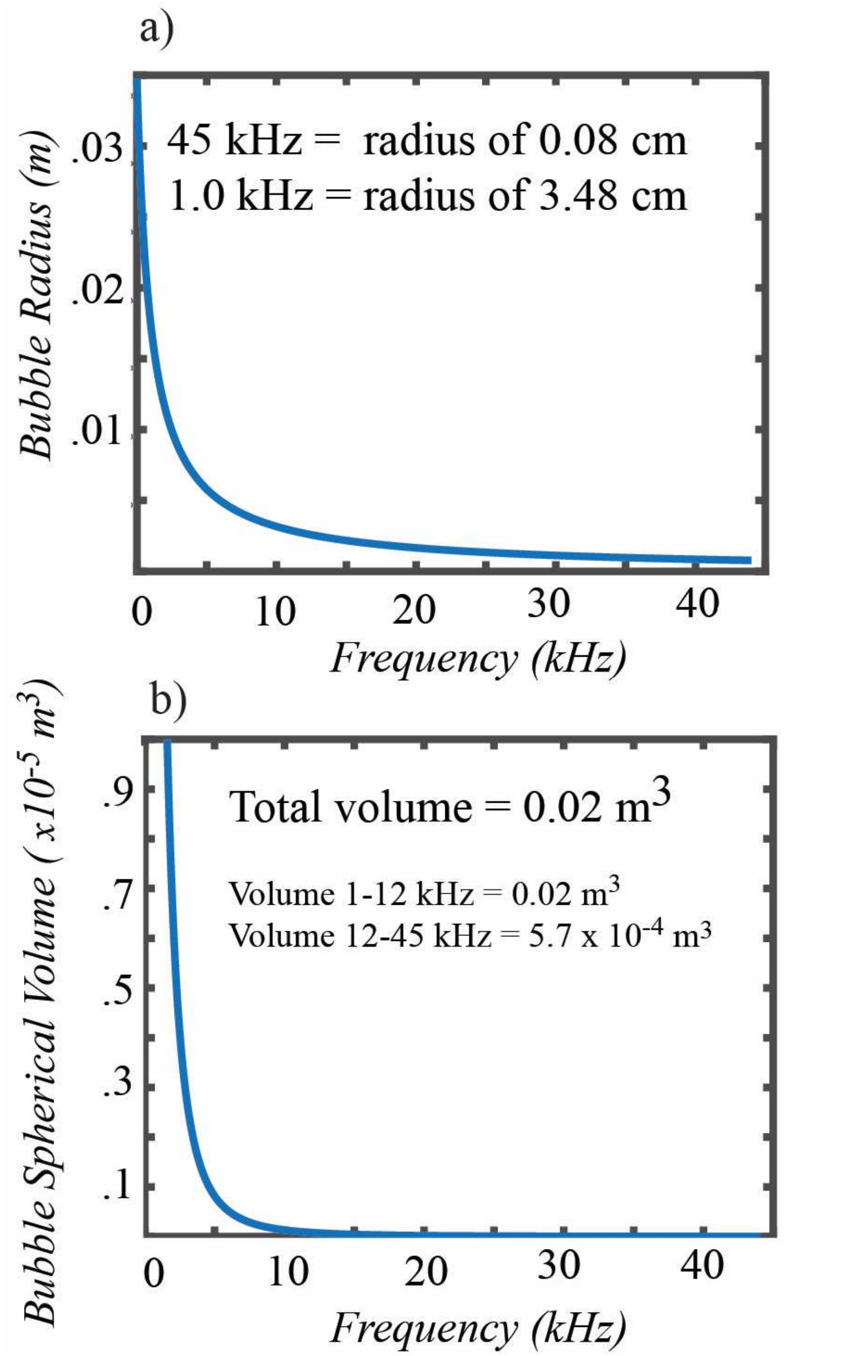

Figure 8: Estimates of bubble radii (a) based on equation (1), and bubble volume (b). The largest values for radius are <20 kHz, becoming asymptotic as the frequency increases to 45 kHz. Bubble volume estimated using bubble radii assuming the bubbles have a roughly spherical volume defined by 4/3 π r^3.